Lawson Spencer, Matthew T. Reiter, Leslie Lok, Sasa Zivkovic

The Finite Element Method (FEM) of the Unlog Tower

Abstract: The Unlog Tower uses finite element analysis (FEA) to simulate the structural, material, and geometric limitations necessary to transform locally available, Emerald Ash Borer (EAB) infested White Ash timbers into bending-active trusses through elastic kinematics. Like other Elastic kinematic structures, the Unlog Tower relies on elastic deformation through inherent material properties to create structurally stable and lightweight bending-active components that can easily be deployed and disassembled. Through robotic kerfing techniques, halved logs are stretched along threaded rods and connected into larger panels with a custom slip washer splice connection. To inform the fabrication of these panels, a finite element method (FEM) was developed to simulate the elastic deformation of individual panels as they were stretched, and a second FEM was developed to test the whole structure against gravity and wind loads. This research uses EAB-infested white ash, to simulate and assemble roundwood timbers into bending-active structural components for a fully permitted outdoor installation.

Keywords: bending active structures, digital timber, deployable structures, finite element analysis, elastic kinematics

1 Introduction

Situated on the Arts Quad at Cornell University in Ithaca, NY, the Unlog Tower (Fig. 1) uses emerald ash borer (EAB) infested White Ash logs in response to the ongoing EAB epidemic (Herms and McCullough 2014). The EAB threatens to eradicate most of the 8.7 billion Ash trees in North America and as of 2018, the epidemic has spread to 35 US states and several Canadian provinces (Flower, Knight, and Gonzalez-Meler 2012; USDA Forest Service 2022). In New York State where ash trees constitute approximately 8 % of the overall tree population, the EAB was first discovered in 2009 (USDA Forest Service 2022). Consequently, many ash trees that were traditionally used for cabinetry, hardwood floors, and baseball bats are now discarded as waste or used as firewood, thereby releasing their carbon store back into the atmosphere. Despite being a locally available timber resource and maintaining their structural properties up to two years after infestation (Persad et al. 2013), ash trees (infected or not) are rarely used in the construction industry. The Unlog Tower expands upon the Unlog method (Lok et al. 2023) to transform EAB infested ash wood logs into a triangular and lightweight timber tower using robotic fabrication, mixed reality (MR) workflows, and augmented reality (AR) instruction.

https://doi.org/10.1515/9783111162683-003

Fig. 1: Unlog Tower. (Photo by Cynthia Kuo)

The Unlog Tower uses EAB infested ash wood logs that would otherwise be discarded as waste, with diameters above 12 inches and lengths between 8, 10, and 12 feet. Such logs fall within standard parameters preferred by regional loggers. By utilizing EAB-infested ash wood as a structurally viable, materially efficient, leaf-spring wall component, the Unlog Tower, challenges present EAB-related logging practices, supply chains, fabrication methodologies, and architectural tectonics as an advocate for the use of EAB infested ash logs in timber construction. The research for the Unlog Tower develops and deploys a Finite Element Method (FEM) to simulate the deformation of individual ash wood boards as they are stretched into leaf-spring panels. Then a second FEM is used to simulate the gravity and wind loads affecting the installation. Both literally and figuratively, the Unlog Tower investigates how far this discarded material resource can be stretched through robotic kerfing and elastic kinematics.

2 Background

In woodworking, kerfing is a relief cut technique that reduces the stiffness of a material, allowing the object to be more pliable through a geometric change (Mansoori et al. 2019). Though, kerfing is often applied to sheet materials to generate surface curvature (Menges 2011), others have kerfed round wood timbers with a track bandsaw, which were then steam bent (Kuo 2022). However, steam bending alters the mechanical properties of wood and thus also weakens the material (Svilans et al. 2019). Controlled elastic deformation through pliable materials is a bending-active method to achieve geometric curvature, while maintaining the structural viability of the material as long as the elastic deformation is reversible (Lienhard et al. 2010). This structural principal is evident in the Multihalle Mannheim built in 1974 and the ReciPlyDome, in which the

timber grid shells were able to elastically deform according to the horizontal translation of the supports until they were pinned in place (Lienhard et al. 2013; Brancart et al. 2017). Within this context, researchers have used finite element analysis (FEA) and other computational physics solvers to simulate the bending of individual plywood panels, which were used for form-finding and fabrication (Schleicher et al. 2015).

Bending-active structures with elastic kinematic joints rely on elastic deformation through material pliability to create structurally stable and lightweight bending-active joints that can be easily stretched and bent (Lienhard et al. 2010; Schleicher et al. 2011). This principle is observed in the Unlog method (Lok, Zivkovic, and Spencer 2023), whereby, roundwood ash logs were robotically cut in half and then kerfed lengthwise to construct a leaf-spring joint between boards for each panel (Fig. 2). The robotic method and leaf-spring structural logic exhibited in Unlog and now, the Unlog Tower is comparable to that of the Torus Research Pavilion by CODA, in which individual plywood boards were face coupled with rigid connections allowing the boards to elastically deform when stretched (Tornabell, Soriano, and Sastre 2014). The Torus assembly was flat-packed and quickly unraveled on site to exhibit and validate the inherent bending-active structural principles of the plywood members. Both Torus and Unlog investigate the fabrication feasibility of bending-active, leaf-spring timber structures through their respective elastic kinematic assemblies. Instead of relying on a sheet material, the Unlog method unravels the volumetric roundwood into an operable leaf-spring component as opposed to assembling individual sheets that are then unraveled. By doing so the Unlog method attempts to reduce the amount of waste material produced through squaring of a log for dimensional lumber and/or reducing the amount of adhesive required for plywood. In this way, the robotically kerfed roundwood components produced through the Unlog method can easily be recycled at the end of use.

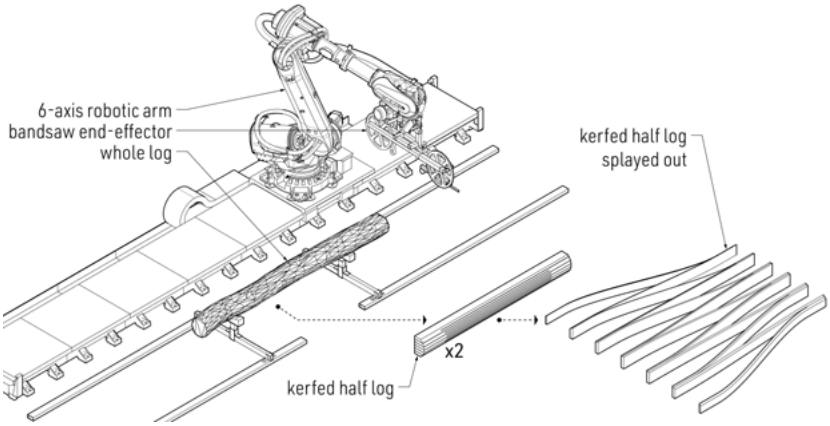

Fig. 2: Robotic kerfing diagram.

3 Methods

FEA is not only used to analyze the effects of gravity and wind loads on the pavilion, but also simulate the displacements of individual half logs (panels) as they stretch along two threaded rods into panels. This simulation is used to inform the robotic fabrication of each individual half log. In response to the ongoing EAB epidemic, the Unlog Tower uses EAB infested ash logs which maintain their structural properties for two years after infection (Persad et al. 2013). The research methods will present the following: the structural principals and code limitations that are used to inform the overall design (Sec. 3.1), the design of the foundation connection (Sec. 3.2), the difference between geometric curvature and elastic bending (Sec. 3.3), the design of the splice connection (Sec. 3.4 and its relation to the robotic fabrication and coordination (Sec. 3.5), with mention of the design of the tube steel frames (Sec. 3.6). Finally, the methods will conclude with illustrations of the parameters defining the analytical model for FEA (Sec. 3.7). The results of these methods will illustrate the displacements due to wind and gravity loads as well as additional coordination models developed from the FEM. The work presented demonstrates a FEM method to simulate and assemble EAB-infested roundwood timbers into a fully permitted outdoor tower installation through elastic kinematics.

3.1 Code Limitations and Design

The driving geometry from which the Unlog Tower is developed from the structural principals of a triangular column, a triangular prism. Based upon the Euler buckling formula below, the triangular prism has a critical buckling load (P_{cr}) of 1.2 times that of cylindrical prism and almost 1.2 times that of the rectangular prism (Sandaker, Eggen, and Cruvellier 2011).

$$P_{cr} = \pi^2 EI/l^2$$

This observation assumes that between the three prismatic columns, the elasticity of the material (E), the length of the column (l), and the cross-sectional area (A) for the moment of inertia (I) are all constant (Sandaker et al. 2011). For the design of the Unlog Tower, the base of the triangular prism was to be accessible with a $60''$ wheel chair turning diameter in accordance with the standards set by the American Disability Act (ADA) (DOJ and DOT 2014, Sec. 304.2.1). Additionally, the entry was to have a minimum clear opening of $32''$ with no more than a $4''$ projection into either side of the opening between $34''$–$80''$ from the ground (DOJ and DOT 2014, Sec. 404.2.3). These codes informed the design of the entry openings at the base of the installation (Fig. 3).

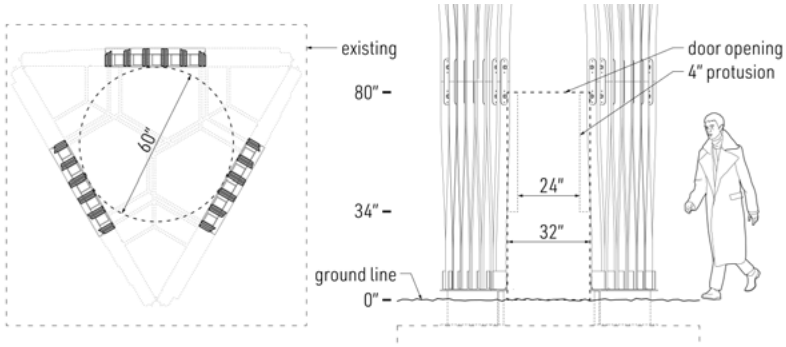

Fig. 3: Unlog Tower plan with ADA design parameters.

3.2 Foundation Connection

The openings at the base led to the design of the foundation design. This particular location on the Cornell Arts Quad had a buried concrete foundation from a previous art installation (Chong 2015). The foundation connection to the timber consisted of three steel I-beams (W14 × 30) that were secured to the concrete pad with eight $0.5''$ diameter threaded rods per I-beam. Each threaded rod went $6''$ deep into the foundation and was secured with an epoxy adhesive. Sitting atop the I-beam was a steel angle ($L5 \times 5 \times 0.25''$), welded on one side of the I-beam and bolt fastened on the other. Atop the steel angle, seven $0.25''$ steel plates were welded to the angle with two $0.875''$ holes in each. The six $1.5''$ wide wood boards were bolted to these plates with 5 steel angles ($L7 \times 4 \times 0.375''$). This detail fixed translation in the local x, y, and z axis and resisted rotation around the local x and y axis, but not the z axis (Fig. 4). This relation was used to define the supports in the analytical model for FEA.

3.3 Geometric Curvature vs. Elastic Bending

Based upon geometric studies conducted in Rhino3D and Grasshopper (Robert McNeel & Associates 2022; Rutten 2022), it was known that if boards were spaced evenly along a threaded rod, the total height of the panel would decrease with respect to the spread distance. Additionally, if the bounding shape was a trapezoid as opposed to a rectangle, the boards towards the end would be longer than the boards in the center to have a parallel top and bottom for the threaded rods to pass through (Fig. 5). In Fig. 5, the change in board length per each panel is represented through a green to yellow to red gradient with Δl (delta length) as the total change in length between boards per panel. The change in length was defined to ensure the top and bottom edges of the panel were parallel for the threaded rods to pass through.

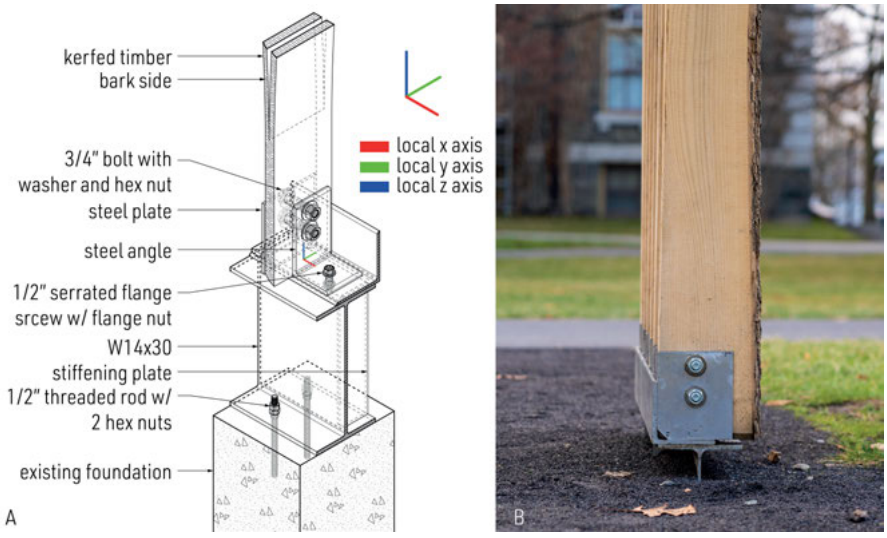

Fig. 4: Foundation Connection: (A) axonometric of foundation detail with support definition; (B) Photo of Ground Connection. (Photo by Cynthia Kuo)

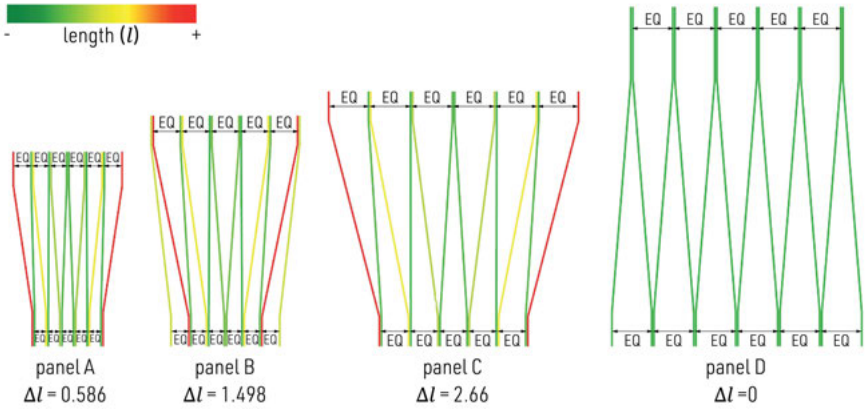

Fig. 5: Change in board length for trapezoidal panels (A-C) and rectangular panels panel D.

The curvature per board was initially assumed through the geometric construction of a Bezier curve which respected the board length relative to the stretching of the before-mentioned panels. However, through prototyping it was revealed that the actual board curvature from elastic deformation in the physical prototype was different than the assumed curvature based upon the Bezier curve construction. This issue affects the ability of the threaded rods to pass through the kerfed panel without bending. In order to simulate the actual bending and determine the length of each individual board more accurately, a FEM was developed to measure the elastic deformation of each individual

panel as it was being stretched (Fig. 6). In this FEM, two fixed points were placed at the center-most board; all other boards could transition in the local *x* and *y* axis. Four-point loads were applied to the outer most boards on the top and bottom of the kerfed log.

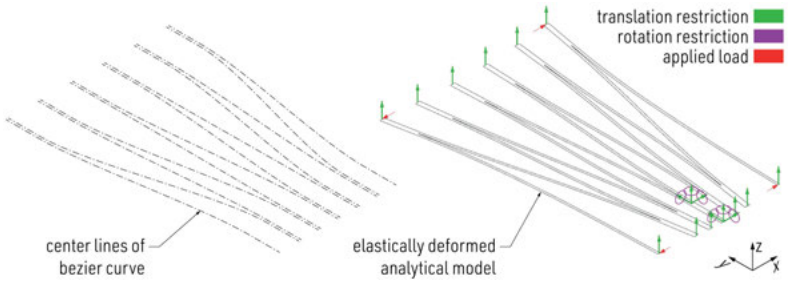

Fig. 6: Comparison between Bezier stretched model and elastic deformation model.

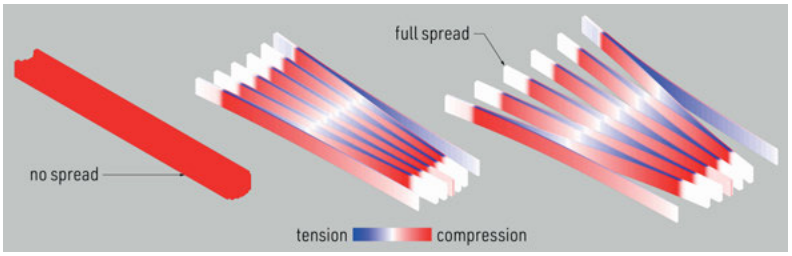

Fig. 7: Individual trapezoid panel being spread through FEA.

Curvature through geometry idealizes a particular material condition, whereas curvature designed through the simulated elastic properties of the material enables the geometry to adapt to a probable or likely condition, which is critical when integrating other connected assemblies. Both Fig. 6 and 7 describe this relationship, which was simulated in Karamba3d, a parametric FEA solver for Rhino3d and Grasshopper (Preisinger and Heimrath 2014). In this FEM, individual boards were defined as shells (meshes) whose orientation followed that of the wood grain. According EN 1912 (2012), White Ash, Fraxinus americana, falls under the Eurocode strength class D35; the material properties in the FEA were based upon such. A single point load was applied to the top and bottom edges of each board, which when increaded, stretched the kerfed log panel. The model was analyzed with the first order theories of small displacements (Rubin and Schneider 2002). The first-order theory assumes that the deflection of the shell is in-line with the mesh face orientation for orthotropic materials and that the cross-sections of the shells remain planar through deformation. This FEM effectively demonstrated how

the robotically kerfed half logs would stretch, given the applied forces. This simulation was used to help stagger the finger joint location within each half log so that the top and bottom edges of each panel would be parallel when stretched.

3.4 Splice connection

The splice connection joins individual $1.5''$-thick boards together between panels (Fig. 8). As panels are stretched along a $0.875''$ diameter threaded rod with preplaced hex nuts, custom, temporary slip washers are placed between the board and the hex nut to temporarily pin the location of the boards. Each board has a $2''$ diameter hole that the threaded rod with preplaced hex nuts would pass through. This allowed for quick assembly and disassembly of individual panels. Once both top and bottom threaded rods have passed through, panels can be joined together. When panels are joined together, the temporary slip washer is replaced with a custom, plasma-cut steel slip washer with a thickness of $0.25''$. The custom steel slip washer is secured in place with bolts and hex nuts. The finger joints between individual boards allow translation only in the local x axis and allows rotation around the local y and z axis. In the analytical model for FEA, the line joints at the splice connection assume no local translation and only rotation around the local y and z axis. Figure 8b also illustrates the local material orientation between boards, in which the x axis (red axis) is parallel to the wood grain.

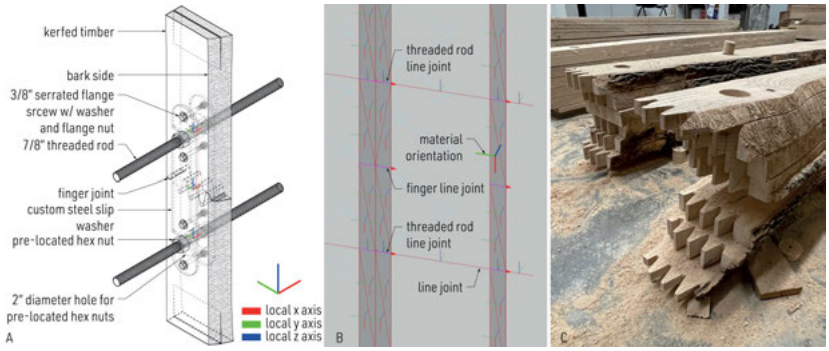

Fig. 8: Splice Connection: (A) detail of splice connection; (B) splice connection in analytical model; (C) Photo of staggered finger joints within a robotically kerfed half log.

3.5 Robotic and Fabrication Coordination

The finger joint location is staggered within the log and different between panels due to the elastic deformation and equal spacing between boards in the three trapezoidal panels. The robotic coordination between individual panels had to ensure (a) that the

bark edge of each panel faced outward from the installation, (b) that the cross-section of each board met the minimum structural requirements, and (c) that finger joint location for both ends of each half log was correctly positioned. To accomplish these three tasks, coordination drawings were made to ensure each half log was correctly positioned in the robot cell. Then the finger joints were cut with an oscillating saw and the holes drilled with a hole saw (Fig. 8c).

3.6 Reciprocal steel frame

Because of the elasticity and diameter of the threaded rods, the tower required interior bracing to keep the sides from bending when exposed to wind loads. Six tube steel frames were designed and fabricated with 11-gauge tube steel to brace the interior of the tower. The tube steel frames were placed in pairs of two between the second and third panel, the third and fourth panel, and at the top of the fourth panel. Each frame was composed of 9 steel tubes with 3 different lengths and a cross section of 3″ by 1″. The interior most connection between 3 tubes was a welded reciprocal frame and the outer three most connections were welded with internal, plasma cut steel plates for added bracing. These 6 frames latched onto the threaded rods that only allowed rotation around the threaded rod axis and the vertical axis of the tube steel cross section.

3.7 Analytical Model

Based upon the detailing and design mentioned in the previous sections, an FEM was constructed that parametrically that related all the translation and rotation restrictions of each joint and support to the joint and support definitions in the analytical model (Preisinger and Heimrath 2014) (Fig. 9). Additionally, a gravity load was applied along with a 100 mph (miles per hour) wind load (Fw) according to the appropriate force to area ratio listed in the ASCE standards 2022. All the material properties for the threaded rods, the tube steel, and the kerfed timber half logs were accounted for, except for the weight of custom steel slip washers in the splice connection. Except for the kerfed timber half logs, all other materials were isotropic and therefore, did not require an added material orientation. The grain orientation for the kerfed logs was accounted for through the mesh face orientation of each board and defined as shell elements in the analytical model. The threaded rods and tube steel were defined as beam elements and the bracing plates between the tube steel members were defined as shells. Finally, a steel plate was placed at the three corner connections between the top two most panels (Fig. 10a). This had the same joint definition as the splice connection (Fig. 10b).

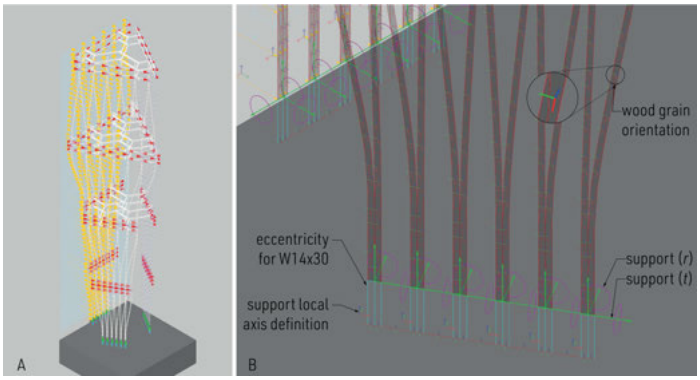

Fig. 9: FEA Model Parameters and Assumptions.

Fig. 10: Left: connection between panels C and D; Right: splice connection. (Photos by Cynthia Kuo)

4 Results

Based upon the reaction forces and reaction moments from the gravity and wind loads at the foundation detail, a force multiplier was created and applied to all loads and calculations in the FEM. The wind loads for were studied from three different directions, perpendicular to a flat face (Fig. 11a), parallel to the same flat face (Fig. 11b), and bisecting a corner condition (Fig. 11c) using the first order theory of small deflections (Rubin and Schneider 2002). The face perpendicular to the flat face proved to have the greatest amount of displacement (d) and was studied for continued displacements, with the following multipliers: $d(0)$, $d(1)$, $d(5)$, and $d(10)$ (Fig. 12). Here the utilization model showed principal compression and tension stress within the structure and was used to evaluate conditions where possible splitting of the wood could take place due to the vertical shear between adjacent boards. The utilization is calculated by taking the total average of the ratio between tension or compressive strengths and the material's comparative stress per mesh face in the case of shell elements and per any point along a curve in the case of beam elements.

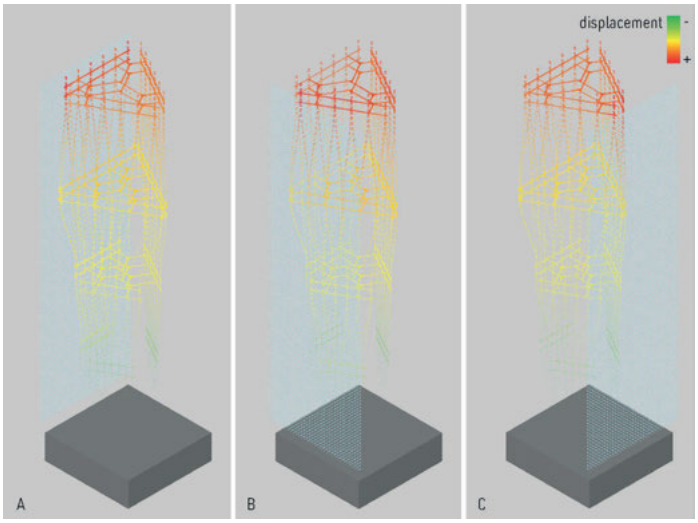

Fig. 11: Tower Displacements per wind load direction. (A) load perpendicular to flat face; (B) load parallel to flat face; (C) load bisecting a corner.

As the design went through several iterations, it became imperative to automate the workflow between design and simulation to quickly communicate the reaction forces at the foundation along with the first and second principal normal forces (Fig. 13a, b), the first and second principal moments (Fig. 13c, d), and the shear forces in the local *x* and *y* directions for the kerfed timber members (Fig. 13e, f). The first principal normal forces were used to check the bearing capacity of each board per mesh face and required reaction force to oppose uplift, while the secondary principal normal forces were used to check for any potential deformation as consequence of the lateral loads. In both cases the compression stresses (red) are negative, and the tension stresses (blue) are positive. Per board, the four highest values for both tension and compression stresses were automatically sorted into a combined list of the extremes for all boards in the model and graphically displayed. The extremes in the combined list were displayed through the red to blue gradient with the highest values being either absolute red or absolute blue in the largest font size. A similar process was repeated for all the moment and shear forces which were displayed through a green to yellow to red gradient. The moment forces in both the first and second directions were checked to see if any board exhibited significant bending, particularly at the unbraced lengths between the bottom two panels. The shear forces, particularly those parallel to the grain, were checked to ensure that there would be no splitting between board members. This simulation greatly assisted in evaluating the complex geometry for locations of overstress and enabled an iterative design process. Finally, if the board lengths in the digital model did not match those fabricated, as would have been the case if they were constructed

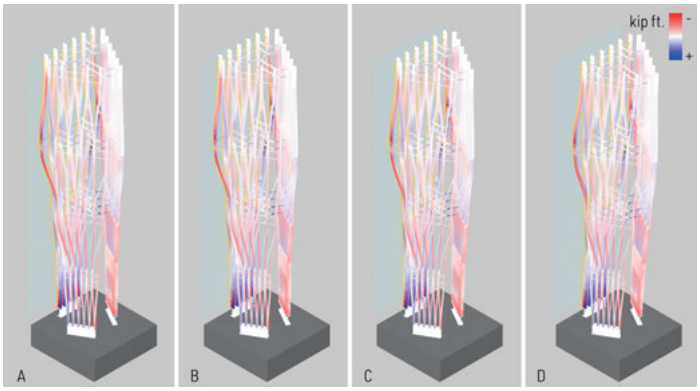

Fig. 12: Tower displacements *d* per wind and gravity loads: (A) $d \cdot 0$; (B) $d \cdot 1$; (C) $d \cdot 5$; (D) $d \cdot 10$.

through Bezier curves, then the change in length between members would have created added shear in the splice connection and potentially splitting as a consequence.

5 Conclusion

The FEM developed for the Unlog Tower was used both graphically and empirically to quickly coordinate between architectural design iterations and structural engineering. Ultimately, the collaboration between the two led to the submission and acceptance of a permitted building set for this installation with an engineer's stamp of approval. Each of the four different panels were assembled into one long prefab panel; this process was repeated twice more until all three sides of the tower were prefabricated. The installation was assembled on its side and then lifted into place with a boom forklift. During the lifting process, the topmost tube steel frame broke in transportation to the foundation pad, due to initially inadequate rigging. The finite element model was re-run to see whether or not the broken tube steel needed to be replaced. The simulation proved viable without the added bracing, and the tower was installed with one less reciprocal steel frame. The tower remained in service for seven months and performed as anticipated through winter conditions.

This research demonstrated how to stretch EAB infested timbers into a structurally viable wall assembly through bending-active elastic kinematics, which were simulated through the development of a custom FEM. The methods illustrated how the design of the structure was informed by code, which lead to the design of the foundation detail. This was followed by assumptions of Bezier curves compared to bending-active bending boards simulated through FEA, which lead to the design of the splice connection. To successfully assemble the trapezoidal panels according to the detail a custom robot coordination workflow was developed, which was followed by the design and detail of

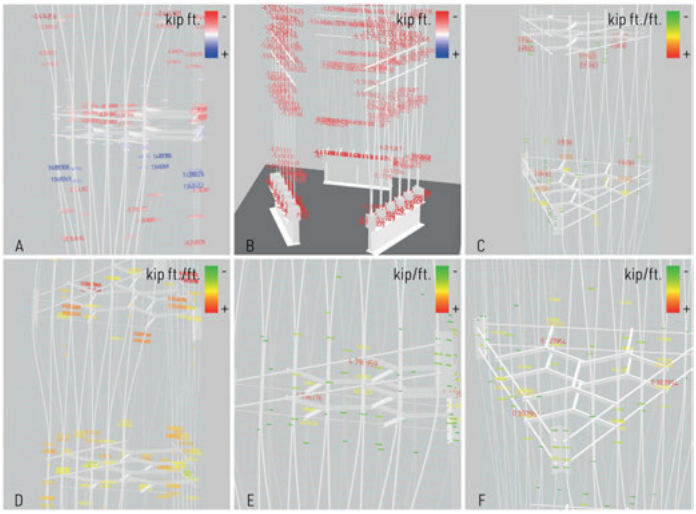

Fig. 13: Graphic display of forces for structural coordination: (A) first principal normal forces; (B) second principal normal forces; (C) first principal moment forces; (D) second principal normal forces; (E) shear force parallel to wood grain; (F) shear force perpendicular to wood grain.

several tube steel framed to brace the interior of the pavilion. Finally, all the design of all the joints and supports were defined in analytical model for the FEA. The FEM developed through this paper was used graphically and empirically coordinate between architectural design and structure. From the development of the FEM to the building approval process, to the successful install and performance (in service), the Unlog Tower demonstrates the viability of EAB infested ash wood as a novel bending-active leaf spring wall panel through FEA.

References

ASCEE. 2022. *Minimum Design Loads and Associated Criteria for Buildings and Other Structures*. Vol. 7–22. ASCE Standard. American Society of Civil Engineers.

Brancart, S., O. Larsen, L. De Laet, and N. Temmerman. 2017. Bending-active reciprocal structures based on equilateral polyhedral geometries. In *Proceedings of the IASS Annual Symposium 2017,* eds. A. Bögle and M. Grohmann.

Chong, Jaeho. 2015. A Needle Woman: Galaxy Was a Memory, Earth Is a Souvenir. *Space,* 114–18.

Department of Justice (DOJ), and Department of Transportation (DOT). 2014. U.S. Access Board - ADA Accessibility Standards (Enhanced Single File Version). https://www.access-board.gov/ada/.

European Committee for Standardization. 2012. EN1912: Structural Timber – Strength Classes – Assignment of Visual Grades and Species.

Flower, C. E., K. S. Knight, and M. A. Gonzalez-Meler. 2012. Impacts of the Emerald Ash Borer (Agrilus Planipennis Fairmaire) Induced Ash (Fraxinus Spp.) Mortality on Forest Carbon Cycling and Successional Dynamics in the Eastern United States. *Biological Invasions 15* (4): 931–44.

Herms, D. A., and D. G. McCullough. 2014. Emerald Ash Borer Invasion of North America: History, Biology, Ecology, Impacts, and Management. *Annual Review of Entomology* 59 (1): 13–30. DOI: 10.1146/annurev-ento-011613-162051

Kuo, E.-K. 2022. The eco bend steam-lam tree log. Now design spotlight. 2022. https://drivenxdesign.com/d100/project.asp?ID=16434

Lienhard, J., H. Alpermann, C. Gengnagel, and J. Knippers. 2013. Active Bending: A Review on Structures Where Bending Is Used as a Self-Formation Process. *International Journal of Space Structures* 28 (3–4): 187–96. DOI: 10.1260/0266-3511.28.3-4.187

Lienhard, J., S. Schleicher, J. Knippers, S. Poppinga, and T. Speck. 2010. Form-Finding of Nature Inspires Kinematics for Pliable Structures. In *Proceedings of the International Symposium of the International Association of Shell and Spatial Structures (IASS),* 2545–54. Spatial Structures – Permanent and Temporary. Shanghai, China.

Lok, L., S. Zivkovic, and L. Spencer. 2023. UNLOG: A Deployable, Lightweight, and Bending-Active Timber Construction Method. *Technology|Architecture + Design* 7 (1): 95–108. https://doi.org/10.1080/24751448.2023.2176146.

Mansoori, M., N. Kalantar, T. Creasy, and Z. Rybkowski. 2019. Adaptive Wooden Architecture. Designing a Wood Composite with Shape-Memory Behavior. In *Digital Wood Design: Innovative Techniques of Representation in Architectural Design,* ed. F. Bianconi and M. Filippucci, 703–17.

Menges, A. 2011. Integrative Design Computation: Integrating Material Behaviour and Robotic Manufacturing Processes in Computational Design for Performative Wood Constructions. In *Proceedings of the 31st Annual Conference of the Association for Computer Aided Design in Architecture (ACADIA),* 72–81. ACADIA 11: Integration through Computation. Banff, Alberta: ACADIA.

Persad, A. B, J. Siefer, R. Montan, S. Kirby, O. J. Rocha, M. E. Redding, C. M. Ranger, and A. W. Jones. 2013. Effects of Emerald Ash Borer Infestation on the Structure and Material Properties of Ash Trees. *Arboriculture and Urban Forestry* 39 (1): 11–16.

Preisinger, C., and M. Heimrath. 2014. Karamba—A Toolkit for Parametric Structural Design. *Structural Engineering International* 24 (May).

Robert McNeel & Associates. 2022. *Rhino3d.* Windows. Robert McNeel & Associates.

Rubin, H., and K. J. Schneider. 2002. *Baustatik: Theorie I. und II. Ordnung.* Werner-Ingenieur-Texte. Werner.

Rutten, D. 2022. Grasshopper. Windows. Robert McNeel & Associates. www.grasshopper3d.com/.

Sandaker, B. N., A. P. Eggen, and M. Cruvellier. 2011. *The Structural Basis of Architecture.* 2nd ed. New York: Routledge.

Schleicher, S., J. Lienhard, S. Poppinga, T. Masselter, T. Speck, and J. Knippers. 2011. Adaptive Façade Shading Systems Inspired by Natural Elastic Kinematics. In *Proceedings of the International Adaptive Architecture Conference IAAC,* 2545–54. London.

Schleicher, S., A. Rastetter, R. La Magna, A. Schönbrunner, N. Haberbosch, and J. Knippers. 2015. Form-Finding and Design Potentials of Bending-Active Plate Structures. In *Modelling Behavior,* ed. M. Ramsgaard Thomsen, M. Tamke, C. Gengnagel, B. Faircloth, and F. Scheurer, 53–63. Springer International Publishing. DOI: 10.1007/978-3-319-24208-8_5

Svilans, T., M. Tamke, M. Ramsgaard Thomsen, J. Runberger, K. Strehlke, and M. Antemann. 2019. New Workflows for Digital Timber. In *Digital Wood Design: Innovative Techniques of Representation in Architectural Design,* ed. F. Bianconi and M. Filippucci, 93–134. Cham: Springer International Publishing. DOI: 10.1007/978-3-030-03676-8_3

Tornabell, P., E. Nadal Soriano, and R. Sastre Sastre. 2014. Pliable Structures with Rigid Couplings for Parallel Leaf-Springs: A Pliable Timber Torus Pavilion. *WIT Transactions on the Built Environment* 136: 117–28.

USDA Forest Service. 2022. Emerald Ash Borer. Emerald Ash Borer Information Network. 2022. http://www.emeraldashborer.info/.